A Concept for Working Point Determination of Axial Compressors Based on Blade Deflection Measurements with Optical Sensors

Rocco Reinhardt*, Daniel M. Lancelle*, Olaf Magnor*, Olaf Hagendorf† and Peter Dünow†
*IAV GmbH, Powertrain Mechatronics, Gifhorn, Germany
Email: rocco.reinhardt@iav.de, daniel.maurice.lancelle@iav.de, olaf.magnor@iav.de,
olaf.hagendorf@hs-wismar.de, peter.duenow@hs-wismar.de
†University of Wismar, Faculty of Engineering, Dept. of Electrical Engineering and Computer Science, Wismar, Germany

***Abstract*—Today, the working point identification of axial compressors is not sufficient, especially of aircraft engine compressors. For this reason, considerable efficiency losses occur in certain working points. The sensors of commonly used measurement methods have to be placed directly in the compressor airflow. This location is not desirable because the sensors are creating vortexes. This paper shows a new method of working point determination of axial compressors. The new developed measurement system with optical sensors provides a contactless blade deflection measurement without influencing the air flow. The assumption is that blade deflections contain information about the actual compressor working point. The advantage of this technique is the minimal invasive nature. Experiments on an axial compressor have approved the assumption and potential of this technique.**

***Keywords*—axial compressor; optical; working point.**

I. Introduction

For many years, strain gauges were usually applied to research blade vibration effects. New methods based on optical sensors have been researched since the 70's [1], [2]. These methods are known as Blade Tip Timing (BTT) or Blade Vibration Monitoring (BVM). In the last fifteen years, the cost for optical equipment, like laser, fast receiver and optical fibers took off rapidly. One of the main reasons for that is the extreme expansion of optical fiber communication. So, optical based blade tip timing is becoming more and more important in compressor research. Other physical sensor principles, like inductive and magneto resistive, microwave or capacitive [3]–[5] are conceivable but they have to show an adequate precision and resolution. The main advantage of BTT is the monitoring of each individual compressor blade with the same sensor set. In addition, BTT do not influence the blades in contrast to strain gauges. With strain gauges, it would be necessary to add them to each blade and implement a telemetry system to monitor them. The time and money invested are extreme in comparison. The tasks in which BTT is most promising currently and in medium term are to extend maintenance intervals on stationary compressors, compressor research in particular stall, flutter and vibration analysis [6]–[8]. A very new approach and still in the beginning of research is the working point determination and optimization [9].

There is a steady development on axial compressors to increase the pressure ratio per stage. This results in a working region which is closer to the non stable state of the axial compressor, the surge line. Currently, accurate working point determination is not possible. To regard the working point uncertainty, the working lines are placed with a greater margin to the surge line. Furthermore, it has to be considered that a compressor aging causes a surge line movement to the working lines. Considerable efficiency losses are the result of these three facts. The sensors of commonly used principles to measure pressure or mass flow have to be placed directly into the air flow. There, they generate vortexes which induce blade vibrations. These vibrations may cause compressor instabilities and so it is not allowed to use intrusive measurement methods. These restrictions lead to uncertainties with working point identifications.

The contribution of this paper is the introduction of a new BTT based working point determination. This method provides a contactless and non-intrusive possibility to detect blade deflections. Aerodynamic effects on compressor blades were analyzed. This analysis leads to the assumption that blade deflections are usable to identify working points. Techniques to prevent or reduce negative influences of engine order (EO) vibrations of blade deflection measurements are presented. To approve the new method, experiments with an axial compressor were done. Therefore, a compressor map was generated to correlate blade deflections with actual working points. These experiments have shown the potential and usability of a working point identification based on blade deflection measurements.

Section 2 describes the aerodynamic effects on the compressor blades to understand the idea of working point identification with blade deflection measurements. Section 3 shows the used measurement principle of BTT to measure blade deflections and also the technical details of the used axial compressor. Section 4 describes preliminary investigations of the compressor blades which allow optimal sensor positioning around the compressor casing. This can prevent or reduce a negative measurement effect because of EO vibration. Section 5 explains the theory of compressor map generation and presents the generated compressor map. Section 6 discusses the reached measurement precision of blade deflection measurements. Furthermore, first measurement results of blade deflections in dependence of the actual compressor working point are presented.

II. Aerodynamic effects on the compressor blade

This section provides a very short insight in the aerodynamic effects on the compressor blades and will help to understand the fundamental idea about working point identification.

Two forces influence the compressor blades during operation, the lift F_{L} and the drag F_{D} (Figure 1). The drag force is the sum of the pressure and the friction force. The lift force is the integral in the direction of the free stream velocity of

 ISBN: 978-1-61208-581-4

the pressure differences between profile top side p_t and profile bottom side p_b for each surface area element dA:

$$F_L = \int_{A_{blade}} (p_t - p_b) \cdot dA \quad (1)$$

It is usual to introduce dimensionless coefficents [10]. The dimensionless coefficient for F_D is:

$$c_D = \frac{F_D}{Aq_\infty} \quad (2)$$

q_∞ is the fluid dynamic pressure and A a defined reference area. For a profile, it is the perpendicular to the ground projected cross sectional area. The dimensionless coefficient for F_L is:

$$c_L = \frac{F_L}{Aq_\infty} \quad (3)$$

These forces are generally generated by the airflow. They are dependent on the airflow velocity C_∞, the profile shape, the Reynolds number, the surface friction, boundary layers, laminar and turbulent flow, et cetera. Further information about these effects are illustrated in technical literature [10], [11].

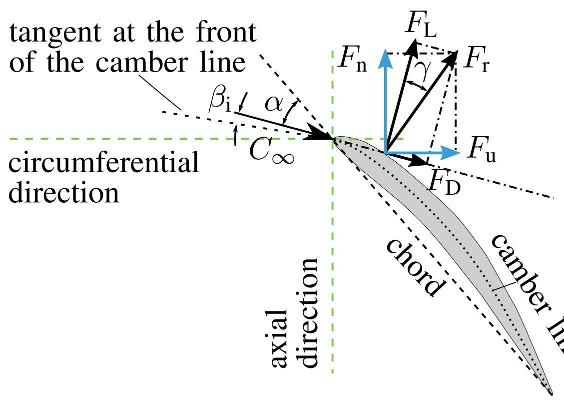

Figure 1. Aerodynamical forces on the compressor blade.

According to the Kutta-Joukowski theorem, the lift force is orthogonal and the drag force is parallel to the direction of flow. F_r is the resulting force. It can be divided into an axial F_n and a circumference force F_u. The angle between the lift and the resulting force is called glide angle γ. The flow direction is described with the angle of attack α. The incidence angle β_i has a major effect on the resulting force. When the compressor is throttled (working point moves left in the compressor map) the pressure ratio increases, the mass flow decreases and the incidence angle increases. Each blade profile shape has a special c_L and c_D behavior depending on the incidence angle [10], [12]. This information can be used to research a working point determination with blade deflections.

III. MEASUREMENT PRINCIPLE AND TECHNICAL DETAILS OF THE AXIAL COMPRESSOR

For the BTT measurement principle, one or several blade sensors are arranged around the circumference of the casing. Figure 2 shows this principle. Alternative sensor positions exist in order to prevent the influence of engine order (EO) vibration amplitudes [6], [7]. When a blade crosses the region of one blade sensor, an event will be created. In the absence of blade bending, it is possible to determine the actual undisturbed position s_0 of each blade in relation to the event of the commonly used OPR sensor or, even better, a high resolution reference system and the actual revolution speed or, rather, period of time. If the blade vibrates in none EO modes, the position varies (s_Δ) with time. Additionally, there will be an offset depending on the working point because s_Δ correlates with the resulting force F_r. The actual blade position of blade w in relation to one reference mark can be calculated with (4).

$$s^w = s_0^w + s_\Delta^w \quad (4)$$

$$w : [1, \text{h=Number blades}] \text{ with } w \in \mathbb{Z}$$

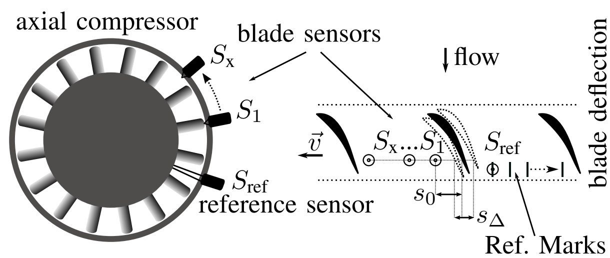

Figure 2. BTT measurement principle on an axial compressor.

In this paper, the individual components of F_r will not be regarded, only the effect in circumferential direction. This will be part of further investigations. For this research, a high resolution reference system was used. Several reference marks are mounted on a suitable load independent position, like the shaft or the disk. They are triggering events at constant angles of the compressor turn. The essential velocity or period of time is calculated with the time difference between two reference events. More details and strategies for a high resolution reference and blade position determination are illustrated in [13].

For the investigation of compressor effects and achievable precisions, a set of three optical blade sensors and one reference sensor is used. Figure 3 shows the principle of the blade sensors. There is one coupling fiber with a core diameter of 4 μm and one outcoupling fiber with a core diameter of 102 μm. Both fibers are guided over a combiner module to one integrated transmitting and receiving end. The combined end has a long ferrule to overcome the width of the compressor casing. The reference sensor is built similarly, except for the ferrule. A ferrule connector for physical contact (FC/PC connector) is used instead. The beam from a laser source with a wavelength of $\lambda = 780\ nm$ and a power of 20 mW is coupled into the sensor module. When the radiated light from the transmitting fiber is reflected by an object, like a blade or a reference mark, the reflected light is collected by the receiving fiber and then guided to an optical receiver. The receiver converts the optical to an electrical signal. A digital storage oscilloscope is used to acquire the data for the following data analysis. Considering that the differences of blade deflections in several working points are often in the range of micrometers, that makes it necessary to regard negative effects, like time walk and time jitter. [14] describes these effects and methods to reduce them. The complete measurement system runs with a sampling rate of $f_s = 250\ MHz$ with a 3 dB bandwidth of approximately $f_{BW} = 200\ MHz$.

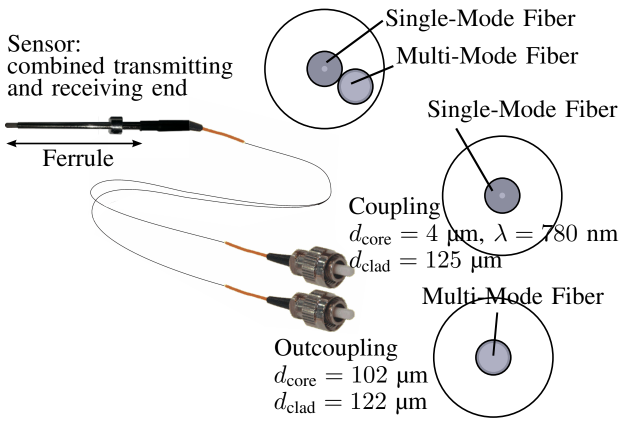

Figure 3. Optical blade sensor setup with special ferrule.

The axial one stage intermediate-pressure-compressor with the internal name EB52 has $h = 58$ blades. It is a research compressor at the Whittle Laboratory of the University of Cambridge and is driven by a synchronous motor to a maximum revolution speed of $n = 3000\ 1/min$. The inner diameter from blade tip to blade tip is $d_c = 0.487\ m$. The compressor can reach an aerodynamic power of about 6 kW and a pressure ratio of $\Pi = 1.02$. The pressure ratio of this research compressor is in comparison to civil engines very small. The engine PW6124 (Airbus A318) from Pratt & Whitney reaches $\Pi = 1.83$ per stage [10]. The one stage compressor HP9 (report AGARD-AR-275) reaches $\Pi = 1.24$. Additionally, the blades of EB52 are very stiff in relation to the maximum aerodynamic power and pressure ratio, so that the blade deflections will be relatively small.

IV. Preliminary Investigation of Axial Sensor Positioning

Usually, blade vibrations f_{blade} have a random character with small amplitudes, thereby averaging is permissible. But, sometimes, varying tip clearances or stator parts lead to excitation of the blades natural frequencies and the vibration amplitudes are rising. For the quality of BTT measurement, this is adverse in the case of EO vibrations. An EO vibration is an integer multiple of the revolution frequency f_{rev} (5).

$$EO = \frac{f_{blade}}{f_{rev}} \text{ with } EO \in \mathbb{Z} \tag{5}$$

If the compressor blades vibrate with this kind of frequency, the vibration is synchronized with the compressor revolution. Figure 4 shows a blade vibration with an EO of 6 (blue line). It is defined when the vibration magnitude is negative, the blade comes later to a sensor position because the vibration direction is opposite to the rotational direction. When the magnitude is positive, the blade comes earlier to a sensor position. The sensor positions are called disturbed positions for both states. Only vibration nodes represent undisturbed sensor positions and are usable for direct blade deflection measurements. Furthermore, the blue line can be interpreted as the delta arrival time caused by an EO blade vibration for imaginary sensor positions. If the sensors are located on disturbed positions around the compressor circumference, the measurement result shows a false static blade deflection. If EO vibrations are not considered, blade deflection measurements for working point determination or vibration analysis for flutter or stall may be difficult or impossible. Therefore, one of the main tasks for BTT is an optimal sensor positioning.

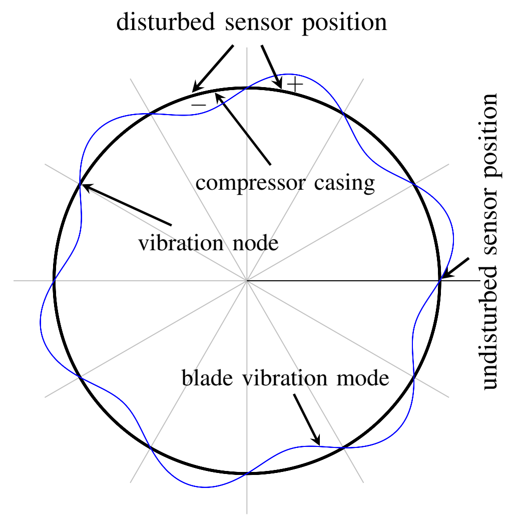

Figure 4. Engine order blade vibration.

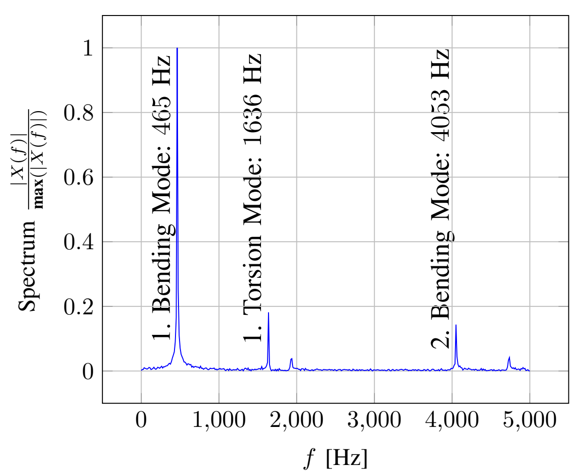

Figure 5. Blade vibration eigenfrequency and eigenform analysis.

The compressor blades were surveyed and the eigenfrequencies (natural frequencies) and eigenforms were identified. Figure 5 shows the resulting frequency spectrum and most significant frequencies. The mode shapes with the most influence on BTT measurement were analyzed in detail.

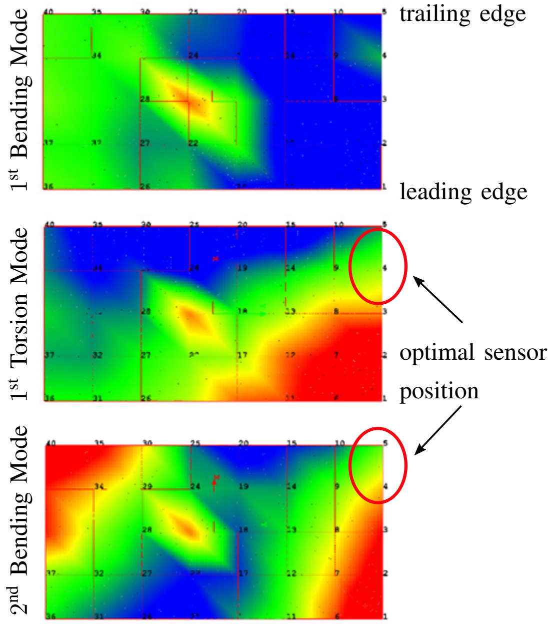

Figure 6. Axial sensor positioning with blade vibration analysis, green region stands for vibration node.

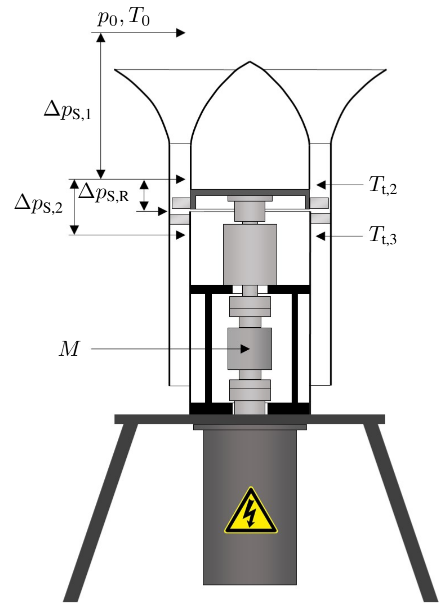

Figure 7. Overview of the probe positions of the test rig.

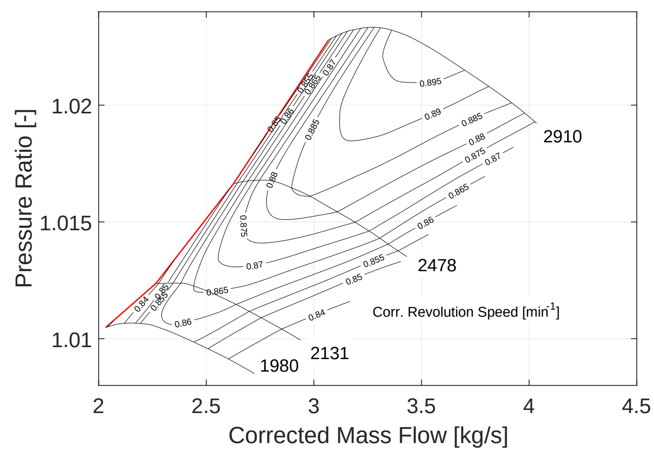

Figure 8. Compressor map for the EB52.

Figure 6 reveals that the 1st torsion and 2nd bending mode show nodes of vibration close to the trailing edge. This effect is used to minimize their influence to blade deflection measurements for working point determination. The sensors are positioned close to the trailing edge. In the case of EO blade vibration with 1st torsion or 2nd bending mode, they should not affect the measurement. The 1st bending mode shape makes it impossible to use an ideal sensor position. Unfortunately, this mode has the biggest amplitude.

V. COMPRESSOR MAP GENERATION

To correlate the acquired blade deformation data to the corresponding working points, all important measurement values need to be recorded. One sample of specific values describes a specific working point. All working points span the compressor map which describes the physical behavior of the compressor. The test rig is equipped with a data acquisition system which measures the revolution speed n, the torque at the shaft M, the static inlet temperature T_0, the total temperature upstream of the rotor $T_{t,2}$, the total inlet pressure $p_{t,0}$, the pressure difference between inlet and the rotor $\Delta p_{S,1}$ and the differential pressure over the compressor stage $\Delta p_{S,2}$. With these values, the compressor map can be determined. Detailed information about compressor map generation are illustrated in [10]. Additionally, the pressure difference over the rotor $\Delta p_{S,R}$ as well as the total temperature downstream of the stage $T_{t,3}$ are measured. Figure 7 shows the probe positions of the test rig.

Figure 8 shows the generated compressor map for the axial compressor presented in this paper.

From the inlet conditions and the pressure drop between inlet and rotor $\Delta p_{S,1}$ the mass flow $\dot{m}$ can be derived. The pressure difference over the stages $\Delta p_{S,2}$ enables to determine the pressure ratio Π of the compressor. The power at the shaft P_{in} is computed from the torque M and the revolution speed n. The mass flow and the pressure ratio allow the calculation of the required power for the pressure rise under isentropic conditions P_{id}. The ratio of the isentropic and the measured power yields to the compressor efficiency η. To create the compressor map, the compressor is throttled until it stalls. The pressure ratio is plotted versus the mass flow for different rotational speeds. Based on the measured efficiency, a contour plot is created to show lines of constant efficiency. As the compressor's behavior is dependent on the inlet conditions, it is not convenient to use the real mass flow and rotational speed, as the compressor map would not be the same on two different days or two different altitudes. Hereinafter, the different conditions are described with I and II. Therefore, the

 ISBN: 978-1-61208-581-4

compressor map is transformed in a way that every point in the map has its specific streamline pattern. This can be achieved if the Mach number in axial (Ma_{ax}) and circumferential direction (Ma_{rad}) are constant for each point in the compressor map. The Mach number in axial direction is:

$$Ma_{\text{ax}} = \frac{c_{\text{ax}}}{a} = \frac{\dot{m}}{\rho A \sqrt{\kappa R T}} \tag{6}$$

with the flow velocity in axial direction c_{ax}, the sonic velocity a, the isotropic exponent κ, the specific gas constant R, the temperature T of the fluid and the corresponding area A [10].

By replacing the density ρ with the law of an ideal gas and subsequently describing the static pressure and static temperature by their total quantities, a constant axial Mach number is achieved when the following equation is satisfied:

$$\dot{m}_{\text{I}} \frac{\sqrt{T_{\text{t,I}}}}{p_{\text{t,I}}} = \dot{m}_{\text{II}} \frac{\sqrt{T_{\text{t,II}}}}{p_{\text{t,II}}} \tag{7}$$

By defining the corrected mass flow as:

$$\dot{m}_{\text{cor}} = \dot{m} \frac{p_{\text{ref}}}{p_{\text{t}}} \sqrt{\frac{T_{\text{t}}}{T_{\text{ref}}}} \tag{8}$$

with the reference values for pressure p_{ref} and temperature T_{ref}. Often, the values of standard atmosphere are used. The total values p_{t} and T_{t} are the values at the compressor inlet.

It is obvious, that a constant axial Mach number is present, when the corrected mass flow is constant. The Mach number in circumferential direction is:

$$Ma_{\text{u}} = \frac{r\omega}{\sqrt{\kappa R T}} \tag{9}$$

Replacing the static temperature with the total temperature and the angular velocity ω with the revolution speed, a constant circumferential Mach number is given when:

$$\frac{n_{\text{I}}}{\sqrt{T_{\text{t,I}}}} = \frac{n_{\text{II}}}{\sqrt{T_{\text{t,II}}}} \tag{10}$$

Introducing the corrected revolution speed:

$$n_{\text{cor}} = n \sqrt{\frac{T_{\text{ref}}}{T_{\text{t}}}} \tag{11}$$

one can see that a constant circumferential Mach number is achieved when the corrected revolution speed is constant. To get a compressor map that is independent of the inlet conditions, the pressure ratio has to be plotted vs. the corrected mass flow. The throttle lines have to be parameterized for constant corrected revolution speeds.

VI. Blade Deflection Results

This section shows the reached measurement precision and discusses the blade deflection results in comparison to the compressor map. Figure 9 shows the single shot resolution θ. The resolution can be calculated with (12). There is v_{t} the tangential velocity, d_{c} the compressor diameter (blade tip to blade tip), f_{rev} the revolution frequency and t_{s} the sampling rate. The single shot resolution is varying from 0.05 μm to 0.26 μm with the actual revolution speed. All other parameters are constant in the equation.

$$\theta = v_{\text{t}} \cdot t_{\text{s}} = \pi d_{\text{c}} f_{\text{rev}} \cdot t_{\text{s}} \tag{12}$$

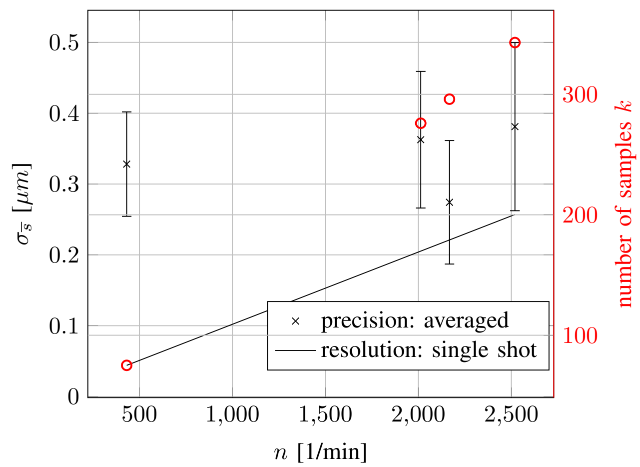

Figure 9. Achieved precision $\sigma_{\bar{s}}$ for all compressor blades, variation $\sigma_{\sigma_{\bar{s}}}$ of precision over all blades and resolution θ of the measurement system.

The resolution is only the first part which describes the quality of a measurement system. The reached precision depending on this resolution is more important. Figure 9 shows also the precision for the distance s^w (4) between a blade w and one reference mark. Each precision value stands for over all compressor blades averaged standard deviation of the arithmetic mean value of each compressor blade. This precision $\sigma_{\bar{s}}$ is calculated with (13):

$$\sigma_{\bar{s}} = \frac{1}{h} \sum_{w=1}^{h} \sigma_{\bar{s}}^{w} \tag{13}$$

with h the number of blades and $\sigma_{\bar{s}}^{w}$ the standard deviation of the arithmetic mean value for blade w.

The arithmetic mean value $\sigma_{\bar{s}}^{w}$ is calculated with (14). σ_{s}^{w} stands for the standard deviation of each individual blade and k for the number of sampled distances s^w.

$$\sigma_{\bar{s}}^{w} = \frac{\sigma_{s}^{w}}{\sqrt{k}} \tag{14}$$

The standard deviation is expressed with (15). For this calculation, the i-th sampled distance s_i^w of blade w to one reference mark and the empirical expected value $\bar{s}^w$ of the sampled distance was used.

$$\sigma_s^w = \sqrt{\frac{1}{k-1}\sum_{i=1}^{k}(s_i^w - \overline{s}^w)^2} = \sqrt{VAR(s^w)} \tag{15}$$

Additionally, in Figure 9 the variation of the standard deviation of the arithmetic mean value over all blades (16) is shown.

$$\sigma_{\sigma_{\overline{s}}} = \sqrt{VAR(\sigma_{\overline{s}}^w)} \tag{16}$$

The precision decreases slightly over the compressor revolution speed and is varying between $0.25\ \mu m$ and $0.4\ \mu m$. The reason for this are the increasing amplitudes of flow induced stochastic blade vibrations. The blades rotate through a steady flow field that is non-uniform in circumferential direction. A forced vibration is induced due to pressure fluctuations.

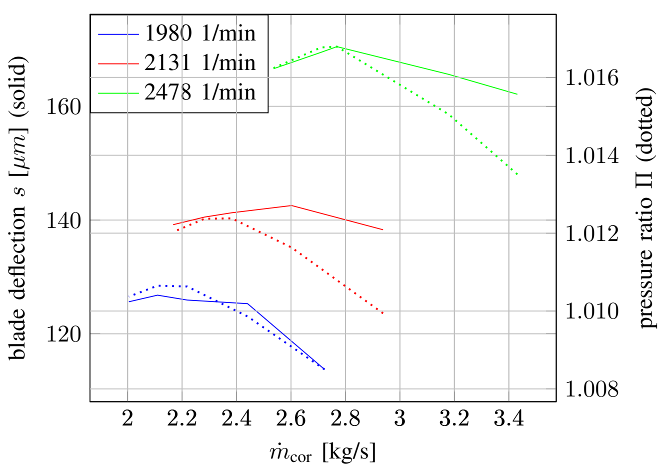

Figure 10. Blade deflection results for several revolution speeds in comparison to pressure ratio Π.

The precision variation of the blades are smaller than $0.125\ \mu m$ and shows the same behavior as the precision. They are increasing with the compressor revolution speed.

Figure 10 shows the first results of averaged blade deflections over the mass flow in comparison with the pressure ratio Π. Each color stands for one corrected revolution speed n_{cor} in the range of $1980..2478\ \frac{1}{min}$. The procedure was to set the revolution speed and change the working point with increasing throttling of the compressor step by step. The increased throttling leads to a reduced mass flow and in the first part to an increased pressure ratio and blade deflection. The working point moves left. Between each step several measurements for the compressor map and the blade deflection were done. The revolution speed lines 1980 and $2478\frac{1}{min}$ show a good correlation to the pressure ratio. The maximum pressure ratio is very closely to the maximum blade deflection. The speed line at $2131\frac{1}{min}$ has another behavior. It could be influenced by undetected EO's, not sufficient measurement quality (poor blade edge quality at this working point), not regarding the individual components of the resulting force F_{r} or another unknown effects.

VII. Conclusion

This paper has introduced a new method of working point identification with blade deflection determination. The theoretical background was explained, the used measurement equipment and several preliminary investigations were presented, and the used statistical values for the analysis were described. The first results were discussed and have proven the possibility of working point identification based on blade deflection measurements. This method allows to increase the efficiency of axial compressors. Further research is recommended to develop more robust sensor principles. It would be desirable to verify this new method on axial compressors with a higher pressure ratio. It is assumed that the measurement effect is much higher there.

Acknowledgment

The authors would like to thank Ivor Day from the University of Cambridge for the interesting professional discussions, the great support and the providing of technical equipment. This research program has been funded by IAV GmbH.

References

[1] I. Zablotskii, Y. A. Korostelev, and L. Sviblov, "Contactless measuring of vibrations in the rotor blades of turbines," DTIC Document, Tech. Rep., 1974.

[2] W. Nieberding and J. Pollack, "Optical detection of blade flutter," in *ASME 1977 International Gas Turbine Conference and Products Show*, American Society of Mechanical Engineers, 1977, V001T01A064–V001T01A064.

[3] M Zielinski and G Ziller, "Noncontact vibration measurements on compressor rotor blades," *Measurement Science and Technology*, vol. 11, no. 7, p. 847, 2000.

[4] P. Procházka and F. Vaněk, "New methods of noncontact sensing of blade vibrations and deflections in turbomachinery," *IEEE Transactions on Instrumentation and Measurement*, vol. 63, no. 6, pp. 1583–1592, 2014.

[5] R. Szczepanik *et al.*, "Application of blade-tip sensors to blade-vibration monitoring in gas turbines," in *Thermal Power Plants*, InTech, 2012.

[6] S Heath and M Imregun, "An improved single-parameter tip-timing method for turbomachinery blade vibration measurements using optical laser probes," *International journal of mechanical sciences*, vol. 38, no. 10, pp. 1047–1058, 1996.

[7] O. Jousselin, *Blade tip timing uncertainty*, US Patent 9,494,491, 2016.

[8] C. P. Lawson and P. C. Ivey, "Tubomachinery blade vibration amplitude measurement through tip timing with capacitance tip clearance probes," *Sensors and Actuators A: Physical*, vol. 118, no. 1, pp. 14–24, 2005.

[9] M. Koeller, O. Magnor, and D. Reitebuch, *Device and method for reliably operating a compressor at the pump threshold*, US Patent App. 13/824,452, 2011.

[10] W. J. Bräunling, *Aircraft Engines, Flugzeugtriebwerke: Grundlagen, Aero-Thermodynamik, ideale und reale Kreisprozesse, Thermische Turbomaschinen, Komponenten, Emissionen und Systeme*. Springer-Verlag, 2015.

[11] H. Herwig, *Fluid Mechanics, Strömungsmechanik*. Springer Vieweg, 2016.

[12] H.-A. Schreiber, W. Steinert, T. Sonoda, and T. Arima, "Advanced high turning compressor airfoils for low reynolds number condition: Part 2-experimental and numerical analysis," in *ASME Turbo Expo 2003, collocated with the 2003 International Joint Power Generation Conference*, American Society of Mechanical Engineers, 2003, pp. 451–463.

[13] R Reinhardt, D Lancelle, O Hagendorf, O Magnor, and P Duenow, "Improved reference system for high precision blade tip timing on axial compressors," in *Optical Fiber Sensors Conference (OFS), 2017 25th*, IEEE, 2017.

[14] R. Reinhardt, O. Magnor, P. Duenow, O. Hagendorf, and A. Rohlfs, "Event detection methods for high resolution time measurements on an application example," in *AUTSYM 2014*, vol. 7, 2014.